Materials Transactions, Vol. 62, No. 6 (2021) pp. 871 to 879
©2021 The Thermoelectrics Society of Japan

Thermal Oxidation Behavior of Magnesium Silicide with Added Alumina or Aluminum

Yoshinobu Nakada*

Central Research Institute, Mitsubishi Materials Corporation, Saitama 330-8508, Japan

Improving the oxidation resistance of Mg_2Si is important for its practical use in thermoelectric devices. The oxidation behavior of Sb-doped Mg_2Si with and without added Al_2O_3 or Al under heating from 293 K to 1023 K in a 200 Pa water vapor atmosphere was observed by using an environmental scanning electron microscope (E-SEM). Compositional analysis before and after *in situ* oxidation in the E-SEM was performed by energy-dispersive X-ray analysis (EDX). The depth profile of the samples after thermal oxidation in the E-SEM was evaluated by X-ray photoelectron spectroscopy (XPS). The dimensionless figure of merit of Sb-doped Mg_2Si with added Al_2O_3 or Al was also evaluated. The oxidation onset temperature was 603 K for Mg_2Si, and 747 K to 793 K for Mg_2Si with 0.8 to 4.5 mol% Al_2O_3 added or 4.0 at% Al added. The O concentration after oxidation at 873 K as measured by EDX (accelerating voltage: 3 kV) was 35.85 at% without Al_2O_3 or Al addition, but 11.55 at% to 13.80 at% with Al_2O_3 or Al addition. The Si concentration after oxidation at 873 K as measured by EDX (accelerating voltage: 3 kV) was 0.30 at% when no Al_2O_3 or Al was added to the Mg_2Si, but 15.32 to 20.97 at% with Al_2O_3 or Al addition. Evaluation by XPS revealed a layer with a relatively high concentration of aluminum oxide or aluminum at a depth of about 20 nm from the surface of the Mg_2Si sample with added Al_2O_3 or Al, respectively. This layer appears to suppress Mg_2Si oxidation. The addition of Al_2O_3 or Al had a slightly positive effect on the thermoelectric properties of Mg_2Si. [doi:10.2320/matertrans.E-M2021812]

(Received July 17, 2020; Accepted March 12, 2021; Published April 16, 2021)

Keywords: *thermoelectric materials, magnesium silicide, alumina, aluminum, oxidation resistance, environmental scanning electron microscope, X-ray photoelectron spectroscopy, thermoelectric property*

1. Introduction

Mg_2Si is an interesting thermoelectric material because it has a higher figure of merit (ZT) in the intermediate temperature range from 500 K to 900 K and is an environmentally friendly and light material. Accordingly, extensive research and development has been carried out with the aim of further improving its thermoelectric properties.[1,2] However, some key challenges remain, including oxidation resistance, which is a major issue for practical use.

Several studies have sought to solve this problem. Tani *et al.*[3] reported that Mg_2Si reacts with O_2 in air to form MgO and Si at 723 K, and that oxidation proceeds via a diffusion-controlled reaction. They proposed a method in which sintered Mg_2Si is coated with β-$FeSi_2$ film to prevent oxygen diffusion at 873 K. Stathokostopoulos *et al.*[4] reported that oxidation begins when the temperature of Mg_2Si exceeds 738 K, and that the rate of oxidation increases above 923 K. They demonstrated that the pack cementation technique helps prevent oxidation of Mg_2Si. Moreover, Battiston *et al.*[5] reported that a 2.5-µm-thick $MoSi_2$ thin-film barrier has good thermo-mechanical compatibility with a sintered Mg_2Si pellet substrate and can provide effective protection up to 873 K. Several effective methods have been proposed in which the surface of Mg_2Si is coated to prevent Mg_2Si oxidation in the intermediate temperature range.[6–8] However, additional methods are needed in order to coat the Mg_2Si surface more easily, efficiently, and evenly. Furthermore, the thermal expansion coefficients of Mg_2Si and the coating materials are not always the same, and thus peeling during long-term use remains a concern. To address these problems, a promising approach is to improve the oxidation resistance of Mg_2Si itself by adding a compound during sintering. In addition, durability would be further improved by applying an oxidation-resistant coating to a material that itself has improved oxidation resistance.

Another issue with Mg_2Si is the strength of Mg_2Si elements. Therefore, this study also investigated the addition of Al_2O_3 to Mg_2Si and evaluated the thermoelectric properties of the prepared samples. Differences were found in surface color and gloss between Mg_2Si with added Al_2O_3 and that without added Al_2O_3. The oxidation resistance of Mg_2Si with added Al_2O_3 was also investigated because its surface was slightly discolored and retained its glossy appearance. To examine the oxidation onset temperature and the corresponding changes in the sample surface, *in situ* oxidation tests were performed using an environmental scanning electron microscope (E-SEM). Differences in experimental conditions for preventing oxidation were investigated by changing parameters such as the amount of added Al_2O_3 and the Sb concentration of the dopant. Furthermore, the mechanism of oxidation suppression in Mg_2Si with added Al_2O_3 was investigated before and after oxidation by quantitative elemental analysis of the surface using energy-dispersive X-ray analysis (EDX), X-ray photoelectron spectroscopy (XPS), and Auger electron spectroscopy (AES). It was found that Al may help suppress oxidation, and therefore the same methods were also used to examine a sample of Mg_2Si with added Al. Finally, the mechanism of oxidation suppression in Mg_2Si with added Al_2O_3 or Al is discussed.

2. Experimental

2.1 Sample preparation

Sb-doped Mg_2Si powder (average particle size 75 µm) containing 0.5 at% Sb or 1.0 at% Sb was purchased from Toshima Manufacturing Co., Ltd. α-Al_2O_3 (product no. ALO11PB, purity 4N, average particle size 1 µm) and Al (product no. ALE11PB, purity 3N, average particle size

*Corresponding author, E-mail: ynakada@mmc.co.jp

本稿は，Materials Transactions, Vol. 62, No. 6 (2021) pp. 871–879 を転載したものである。

3 μm) were purchased from Kojundo Chemical Lab. Co., Ltd.

First, α-Al_2O_3 or Al was added to Sb-doped Mg_2Si powder, and the powder was mixed in a mortar for 15 min. The amounts of α-Al_2O_3 added were 0.8 mol%, 2.3 mol%, and 4.5 mol%, and the amount of Al added was 4.0 at%. These mixed Mg_2Si powders were sintered using an electric current sintering apparatus (SS Alloy Pvt., Ltd.) at sintering pressures of 20 to 40 MPa and sintering temperatures of 1153 K to 1273 K. Sintering was stopped when the displacement rate became almost zero and the displacement became almost constant. As a result, the sintering temperature was not constant because the temperature of initial displacement and the displacement curve depended on the amount and type of additive. The electric current sintering apparatus used is equipped with a carbon heater that heats the side walls, which indirectly heat a carbon jig containing the sample from the outside. The sample size after sintering was about 20 mm in diameter and 9 mm thick.

2.2 Evaluation methods

In situ oxidation measurements were performed using an E-SEM (Quanta450FEG, FEI Co.), and quantitative elemental analysis of the sample surface layer before and after *in situ* oxidation by using an EDX analyzer installed in the E-SEM. The size of the sample used for E-SEM measurements was approximately 1.5 mm × 1.5 mm × 2 mm. The sample was placed in a carbon capsule with inner diameter of about 5 mm and depth of 1 mm. The samples were heated to 873 K or 1023 K at 10 K/min. The samples heated to 873 K were held at that temperature for 10 min and then cooled at 20 K/min; samples heated to 1023 K were cooled immediately at 20 K/min without holding. Heating was performed in a 200 Pa water vapor atmosphere. This pressure was selected considering the incident frequency and the average dwell time of gas molecules on a solid surface. The incident frequency of gas molecules (F) is given by the following equation:

$$F = 2.6 \times 10^{24} p/(MT)^{1/2}$$

where F is the incident frequency of gas molecules ($1/m^2s$), p is the pressure (Pa), M is the molecular weight of gas, and T is the absolute temperature (K).

The F value of 200 Pa water vapor at 773 K is 4×10^{24} $1/m^2s$. The atomic density of the solid surface is about 1×10^{19} atom/m^2. Assuming that all molecules incident on the solid surface are adsorbed, the surface would be completely covered in 3×10^{-6} s. On the other hand, the average dwell time of molecules depends on the activation energy of desorption and the temperature of the solid surface. Because the activation energy of desorption of water molecules on Mg_2Si is not known, the value of 100 kJ/mol for a stainless steel surface was used. From this value and the results in Fig. 11 of Ref. 9), an average dwell time of $\sim 1 \times 10^{-6}$ at 773 K was obtained. As the average dwell time on the solid surface and the time required for incident water molecules to cover it at a partial pressure of 200 Pa at 773 K were roughly on the same order, the heating experiments with E-SEM was carried out in a 200 Pa water vapor atmosphere.

Quantitative elemental analysis by EDX with an electron beam diameter less than 1 μm was performed at the approximate center of each Mg_2Si particle to avoid the effects of grain boundaries and Al_2O_3 aggregated at grain boundaries. Five particles of Mg_2Si were randomly selected, analyzed, and averaged for each sample. In SEM-EDX, Mg, Si, Al, and O were measured at accelerating voltages of both 3 kV and 15 kV, while Sb was measured at only 15 kV because its Kα-Line (3.6 keV) cannot be detected at an accelerating voltage of 3 kV. The analysis area in the depth direction was estimated using the EDX analysis energy table provided by the manufacturer of the instrument (JEOL, Inc). For Mg_2Si, the depth was about 0.2 μm when the accelerating voltage was 3 kV and about 3.5 μm when it was 15 kV.

The depth profiles of Mg, Si, Al, and O in the samples after thermal oxidation were measured by XPS (PHI 5000 VersaProbe 2, ULVAC-PHI Inc.) with Ar^+ ion etching. The X-ray source was Al Kα, and the X-ray beam diameter was 200 μm. The accelerating voltage was 2 kV and the raster size was 2 mm × 2 mm. The amount of Ar^+ ion etching was determined using an oxide film on a silicon wafer, and the etching rate of MgO was assumed to be half that of SiO_2 (internal data).

Particles that formed on the surface after thermal oxidation were analyzed by AES using a PHI 700 scanning Auger nanoprobe (ULVAC-PHI, Inc.). The accelerating voltage was 10 kV, the beam current during secondary electron (SE) image acquisition was 1 nA, and the beam current during analysis was 10 nA.

The electric conductivity and Seebeck coefficient in the range 300 K to 823 K were measured using a ZEM-3 system (ADVANCE RIKO, Inc.) in a decompressed helium atmosphere. The thermal diffusivity and specific heat were measured using an LFA 447 Nanoflash system (Netzsch GmbH) from 300 K to 573 K. From 573 K to 773 K, the thermal diffusivity was measured using a TC-7000 system (Shinku-Riko, Inc.) and the specific heat was measured using a DSC 3500 Sirius system (Netzsch GmbH). Thermal conductivity was determined from the thermal diffusivity, specific heat, and density of sintered Mg_2Si.

3. Results and Discussion

3.1 *In situ* observation of thermal oxidation by E-SEM and elemental analysis using EDX

Figure 1 shows SE images before, during, and after thermal oxidation. Figure 1(a)–(d), (e)–(h), (i)–(l), and (m)–(p) correspond to Mg_2Si (0.5 at% Sb), Mg_2Si (1.0 at% Sb) + 0.8 mol% α-Al_2O_3, Mg_2Si (1.0 at% Sb) + 4.5 mol% α-Al_2O_3, and Mg_2Si (1.0 at% Sb) + 4.0 at% Al, respectively. Figure 1(a), (e), (i), and (m) show the samples before thermal oxidation, (b), (f), (j), and (n) show the samples during thermal oxidation at 707 K, (c), (g), (k), and (o) show the samples during thermal oxidation at 873 K, and (d), (h), (l), and (p) show the samples after thermal oxidation at 1023 K. Grain boundaries were observed in the SE images of all specimens before heating. In particular, the SE images in Fig. 1(e) and (i) clearly show that the added Al_2O_3 agglomerated at the grain boundaries. The added Al was not clearly observed at grain boundaries in Fig. 1(m) because

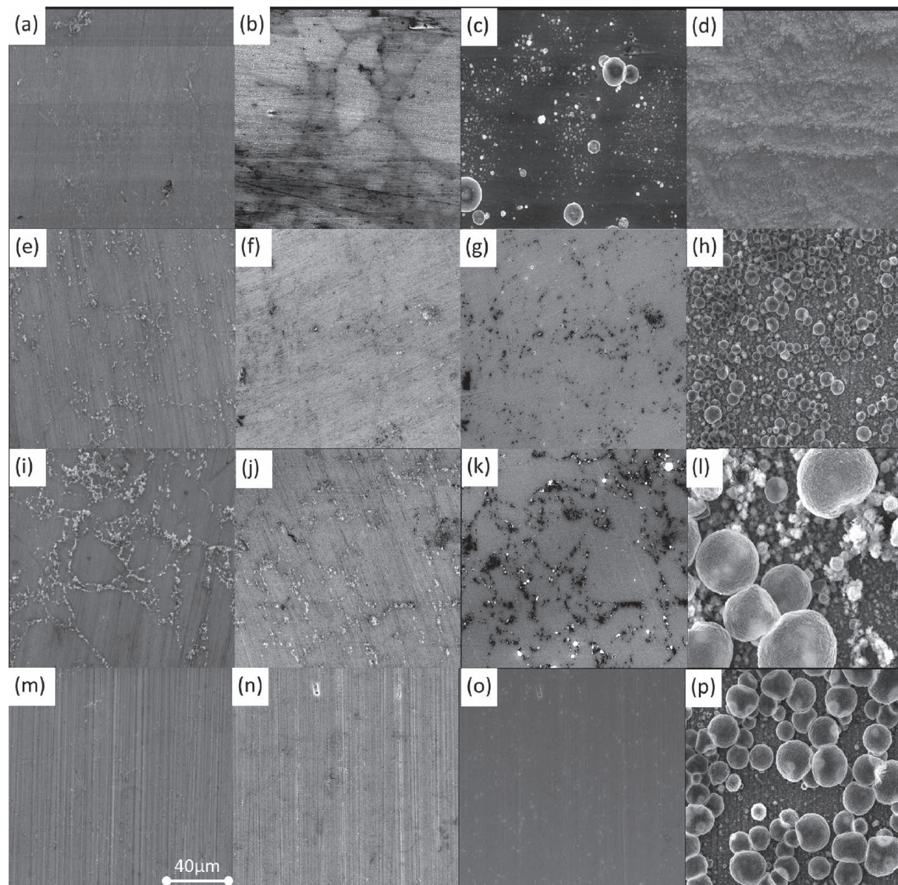

Fig. 1 Secondary electron (SE) images before, during, and after thermal oxidation in a 200 Pa water vapor atmosphere. (a)–(d) Mg_2Si (0.5 at% Sb). (e)–(h) Mg_2Si (1.0 at% Sb) + 0.8 mol% α-Al_2O_3. (i)–(l) Mg_2Si (1.0 at% Sb) + 4.5 mol% α-Al_2O_3. (m)–(p) Mg_2Si (1.0 at% Sb) + 4.0 at% Al. (a), (e), (i), and (m) correspond to before thermal oxidation. (b), (f), (j), and (n) correspond to during thermal oxidation at 707 K. (c), (g), (k), and (o) correspond to during thermal oxidation at 873 K. (d), (h), (l), and (p) correspond to after thermal oxidation at 1023 K.

the sintering temperature of 1247 K is higher than the melting point of Al. In other words, at least some of the Al diffused into the Mg_2Si particles. The SE image in Fig. 1(b) shows that many small particles, which appear as white dots in the SE image, had formed at 707 K on the surface of the sample. However, no clear change was observed in the other images at this temperature. The SE image in Fig. 1(c) shows that the particles grew and some large particles formed at 873 K. Compared with Fig. 1(c), fewer particles formed on the surface of the samples shown in Fig. 1(g), (k), and (o), particularly on those in Fig. 1(g) and (k). However, more particles formed on the surface of the sample in Fig. 1(o) compared with Fig. 1(g) and (k). After thermal oxidation at 1023 K, the surface of the sample shown in Fig. 1(d) was completely covered with many small particles, but no large particles were found in this area. In contrast, the other samples were covered with both small and large particles. Elemental analysis by AES was performed on the small and large particles as shown in Fig. 2. Figure 2(a) shows an SE image of particles formed by thermal oxidation of Mg_2Si (0.5 at% Sb) + 2.3 mol% α-Al_2O_3 at 873 K, and Fig. 2(b) and (c) show the magnified images of the small particle A and the large particle B in Fig. 2(a), respectively. The elemental composition of the small particle A was 58.1 at% Mg, 36.7 at% O, 2.1 at% Al, and 3.1 at% C. That of the large particle B was 57.6 at% Mg, 36.5 at% O, 2.6 at% Al, and 3.2 at% C. These particles were magnesium oxide as revealed by AES. Furthermore, the interior of the large particle B was found to be hollow because it was crushed by Ar^+ ion etching by AES.

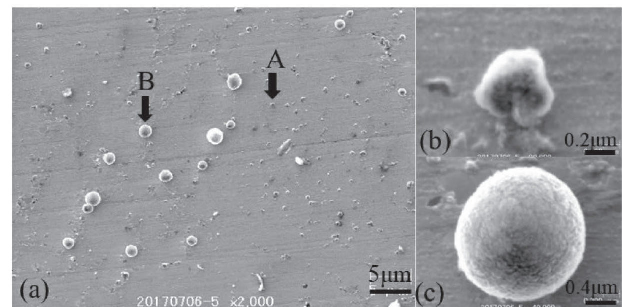

Fig. 2 (a) SE image of particles that formed during thermal oxidation on the surface of Mg_2Si (0.5 at% Sb) + 2.3 mol% α-Al_2O_3 at 873 K. (b) is a magnified image of small particle A. (c) is the magnified image of large particle B.

Figure 3 shows SE images of Mg_2Si (0.5 at% Sb) during heating at (a) 574 K, (b) 603 K, (c) 629 K, and (d) 642 K in a

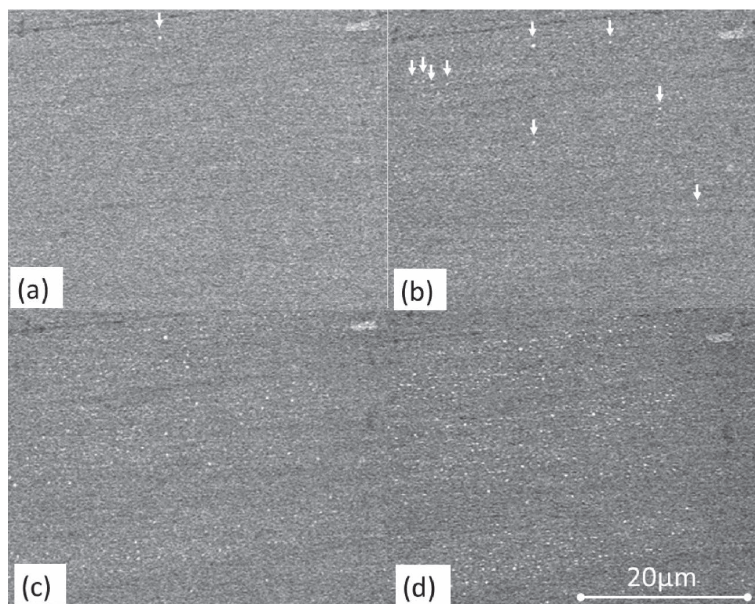

Fig. 3　SE images of Mg_2Si (0.5 at% Sb) during heating at (a) 574 K, (b) 603 K, (c) 629 K, and (d) 642 K in a 200 Pa water vapor atmosphere. White arrows in (a) and (b) show the particles that formed during heating. Many particles (small white dots in SE images) are seen in (c) and (d).

Table 1　Oxidation onset temperature of Mg_2Si observed by *in situ* thermal oxidation.

Sample number	Sample composition	Oxidation onset temperature (K)
1	Mg_2Si (0.5 at% Sb)	603
2	Mg_2Si (1.0 at% Sb) + 0.8 mol% α-Al_2O_3	777
3	Mg_2Si (0.5 at% Sb) + 2.3 mol% α-Al_2O_3*	747
4	Mg_2Si (0.5 at% Sb) + 2.3 mol% α-Al_2O_3**	770
5	Mg_2Si (1.0 at% Sb) + 4.5 mol% α-Al_2O_3	755
6	Mg_2Si (1.0 at% Sb) + 4.0 at% Al	793

* Sintering temperature: 1153 K

** Sintering temperature: 1255 K

200 Pa water vapor atmosphere. A small white particle (white arrow) can be seen in Fig. 3(a) and several small white particles (white arrows) can be seen in Fig. 3(b). Upon further heating, the white dots in the image become progressively sharper and increase in number, as can be seen in Fig. 3(c) and (d). The above AES analysis indicates that the small particles in Fig. 3 are magnesium oxide, and the temperature at which three or more small particles were observed in SE images during heating was defined as the oxidation onset temperature. In the case of Mg_2Si (0.5 at% Sb), the oxidation onset temperature was 603 K. Other samples with added α-Al_2O_3 or Al were also evaluated in the same way and the oxidation onset temperature was determined (Table 1). Samples with α-Al_2O_3 or Al added to Mg_2Si had oxidation onset temperatures of 747 K to 793 K, and that of Mg_2Si samples with added α-Al_2O_3 or Al was higher than that of Mg_2Si samples without added α-Al_2O_3 or Al. Thus, the addition of α-Al_2O_3 or Al to Mg_2Si within the amounts in this experiment helps to suppress the oxidation of Mg_2Si. However, the oxidation onset temperature does not depend on the amount of α-Al_2O_3 or Al added as shown in Table 1. The reason for this will be described later together with the results of compositional analysis before and after oxidation of the sample surface.

Next, differences in the progress of oxidation of Mg_2Si with and without added α-Al_2O_3 or Al were evaluated in more detail by SEM-EDX. Tables 2 and 3 show the results of elemental analysis by SEM-EDX before and after thermal

Table 2 Results of EDX analysis (3 kV) before and after thermal oxidation of Mg_2Si. Oxidation of the sample was carried out at 873 K for 10 min under a H_2O partial pressure of 200 Pa.

Sample number	Before oxidation (at%)				After oxidation (at%)			
	Mg	Si	O	Al	Mg	Si	O	Al
1	64.49	32.19	3.17	0.00	63.85	0.30	35.85	0.00
2	64.52	31.96	3.51	0.02	65.80	20.38	12.26	1.56
3	65.20	32.48	2.08	0.24	69.27	15.32	13.80	1.52
4	65.12	32.37	2.40	0.11	68.97	17.58	12.33	1.12
5	64.63	32.18	3.14	0.05	66.25	20.97	11.55	1.24
6	65.19	32.37	2.42	0.02	66.47	19.83	12.42	1.28

Table 3 Results of EDX analysis (15 kV) before and after thermal oxidation of Mg_2Si. Oxidation of the sample was carried out at 873 K for 10 min under a H_2O partial pressure of 200 Pa.

Sample number	Before oxidation (at%)					After oxidation (at%)				
	Mg	Si	Al	O	Sb	Mg	Si	Al	O	Sb
1	68.23	31.05	0.00	0.49	0.20	63.33	22.31	0.00	14.20	0.16
2	67.84	31.17	0.12	0.54	0.33	67.34	30.52	0.21	1.66	0.33
3	67.28	32.02	0.14	0.36	0.21	67.40	30.61	0.12	1.65	0.22
4	67.00	32.21	0.19	0.40	0.20	66.79	31.59	0.07	1.36	0.19
5	68.26	30.79	0.14	0.49	0.33	67.24	30.93	0.04	1.43	0.36
6	67.56	31.49	0.09	0.46	0.31	68.04	29.88	0.09	1.62	0.31

oxidation at 873 K for 10 min in a 200 Pa water vapor atmosphere at accelerating voltages of 3 kV and 15 kV, respectively. Before thermal oxidation, the concentrations of Mg, Si, and O were almost the same regardless of whether α-Al_2O_3 or Al was added to Mg_2Si. The concentration of Al in Mg_2Si without added α-Al_2O_3 was below the limit of detection, and that in Mg_2Si with added α-Al_2O_3 or Al was 0.02 at% to 0.24 at% at an accelerating voltage of 3 kV and 0.09 at% to 0.19 at% at an accelerating voltage of 15 kV. The Al detected in the Mg_2Si particles was presumably not α-Al_2O_3 aggregated at grain boundaries, for the following reasons. First, EDX analysis with an electron beam diameter of less than 1 µm was performed at the center of each Mg_2Si particle, and no particles suggestive of α-Al_2O_3 were among the analyzed particles. Second, in the Mg_2Si sample without added α-Al_2O_3 or Al, the Al concentration was below the limit of detection.

After thermal oxidation at 873 K for 10 min, the O concentration in the Mg_2Si particles without added α-Al_2O_3 or Al was 35.85 at%, the Mg concentration was 63.85 at%, the Si concentration was 0.30 at%, and the Al concentration was below the limit of detection at an accelerating voltage of 3 kV. However, in the Mg_2Si with α-Al_2O_3 or Al added, the O concentration was 11.55 at% to 13.80 at%, the Mg concentration was 65.80 at% to 69.27 at%, the Si concentration was 15.32 at% to 20.97 at%, and the Al concentration was 1.12 at% to 1.56 at% when measured at an accelerating voltage of 3 kV. When Mg_2Si without α-Al_2O_3 or Al was measured at 15 kV, the O concentration was about 14.20 at%, the Mg concentration was 63.33 at%, the Si concentration was 22.31 at%, and the Al concentration was also below the limit of detection. On the other hand, in the Mg_2Si with α-Al_2O_3 or Al added, the O concentration was 1.36 at% to 1.66 at%, the Mg concentration was 66.79 at% to 68.04 at%,

the Si concentration was 29.88 at% to 31.59 at% and the Al concentration was 0.04 at% to 0.21 at% when measured at an accelerating voltage of 15 kV. From the differences in the analytical values of O concentration and Si concentration between the accelerating voltages of 3 kV and 15 kV, the estimated thickness of magnesium oxide was at least 0.2 µm and less than 3.5 µm in Mg_2Si without α-Al_2O_3 or Al. On the other hand, the estimated thickness of the magnesium oxide in Mg_2Si with added α-Al_2O_3 or Al was less than 0.2 µm. The difference in oxide film thickness is attributed to the presence of a certain concentration of Al in Mg_2Si particles.

The concentration of Al in the sample after sintering Mg_2Si with added α-Al_2O_3 was about 0.1 at% to 0.2 at% for the accelerating voltage of 15 kV, with no clear dependence on the amount of added α-Al_2O_3. This is explained as follows. Al is formed by the reduction of α-Al_2O_3 by Mg at the sites, where Mg_2Si particles and α-Al_2O_3 particles at grain boundaries are in direct contact with each other during sintering. Even if the amount of added α-Al_2O_3 is increased and exceeds a certain amount, the amount of direct contact between the Mg_2Si particles and α-Al_2O_3 particles does not increase. Therefore, the differences in Al concentration in the Mg_2Si samples were small within the range of added α-Al_2O_3 amounts in this work. A plausible reason why there is no clear relationship between oxidation onset temperature and amount of added α-Al_2O_3 or Al is that the difference in Al concentration among Mg_2Si samples is small.

The above results suggest that if about 0.1 at% or more Al is present in Mg_2Si, then its oxidation will be suppressed.

3.2 XPS evaluation of samples after thermal oxidation

Next, to investigate the behavior of the Al concentration in the Mg_2Si in more detail, XPS was used to evaluate the depth profile of Mg, Si, O, and Al concentrations in the sample thermally oxidized at 873 K for 10 min in a 200 Pa water vapor atmosphere using the E-SEM. Because the X-ray beam diameter was 200 µm and the average particle size of Mg_2Si was 75 µm, grain boundary information was included in this measurement. This is why the background concentrations of Al and O were higher than in the SEM-EDX analysis.

Figure 4 shows the depth profile evaluated using Ar^+ ion etching from the surface of Mg_2Si (0.5 at% Sb) to a depth of 275 nm. To this depth, the Si concentration was less than 0.2 at% and the O concentration was almost constant at 45 at% to 50 at%. The Al concentration was about 1 at%, which is probably due to the high background around Al 2p. Therefore, the Al concentration of 1 at% in this XPS depth profile is attributed to the background. Figure 5 shows the depth profile of Mg_2Si (1.0 at% Sb) + 0.8 mol% α-Al_2O_3. The O concentration was almost constant from the surface to a depth of 20 nm, decreased to several atomic percent from 20 nm to 35 nm, and then was almost constant. The Si concentration from the surface to 15 nm was about 1 at%, which was equal to the background level. After that, the Si concentration increased to about 47 at% and became almost constant from 35 nm. The Al concentration increased from 10 nm toward the interior region, reaching a peak at about 25 nm, and then decreased. The peak Al concentration was 6.29 at%. The high Al concentration range was from the point where Si concentration started to increase to just before the Si concentration reached half of its maximum value. The peak Al concentration was located at the depth where the Mg concentration started to increase again after decreasing, before the O concentration began to decrease and the concentration of O became 1/2; furthermore, the Si concentration began to increase before it reached 1/2. The depth profiles of the Mg, Si, O, and Al concentrations in the sample of Mg_2Si (1.0 at% Sb) + 4.5 mol% α-Al_2O_3 were similar to those in Fig. 5. The schematic cross-sectional structure in Fig. 6 shows the structure near the oxidized surface of Mg_2Si with added α-Al_2O_3. In Fig. 6, left side is the oxidized sample surface, A is the MgO layer, B is the

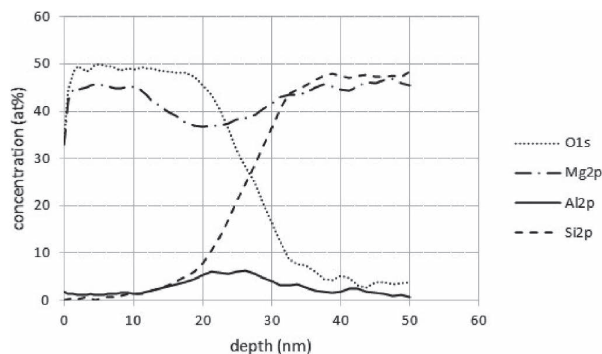

Fig. 5 Depth profile of O 1s, Mg 2p, Al 2p, and Si 2p in Mg_2Si (1.0 at% Sb) + 0.8 mol% Al_2O_3 as observed by XPS.

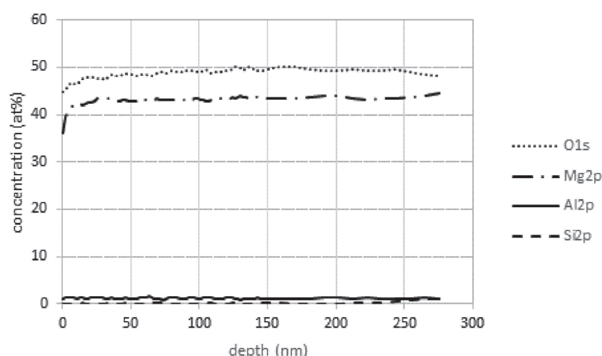

Fig. 4 Depth profile of O 1s, Mg 2p, Al 2p, and Si 2p in Mg_2Si (0.5 at% Sb) as observed by XPS.

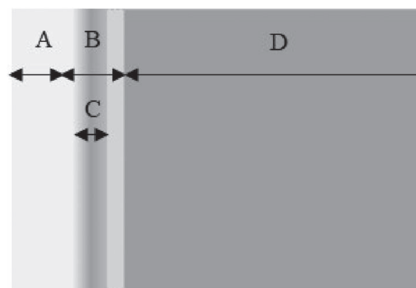

Fig. 6 Schematic diagram of the cross-sectional structure of the sample after oxidation of the Mg_2Si with alumina or Al added. In the figure, the left side is the surface of oxidized Mg_2Si, A is the MgO layer, B is the transition layer between MgO and Mg_2Si, C is the segregated layer of aluminum oxide and aluminum, and D is the Mg_2Si matrix.

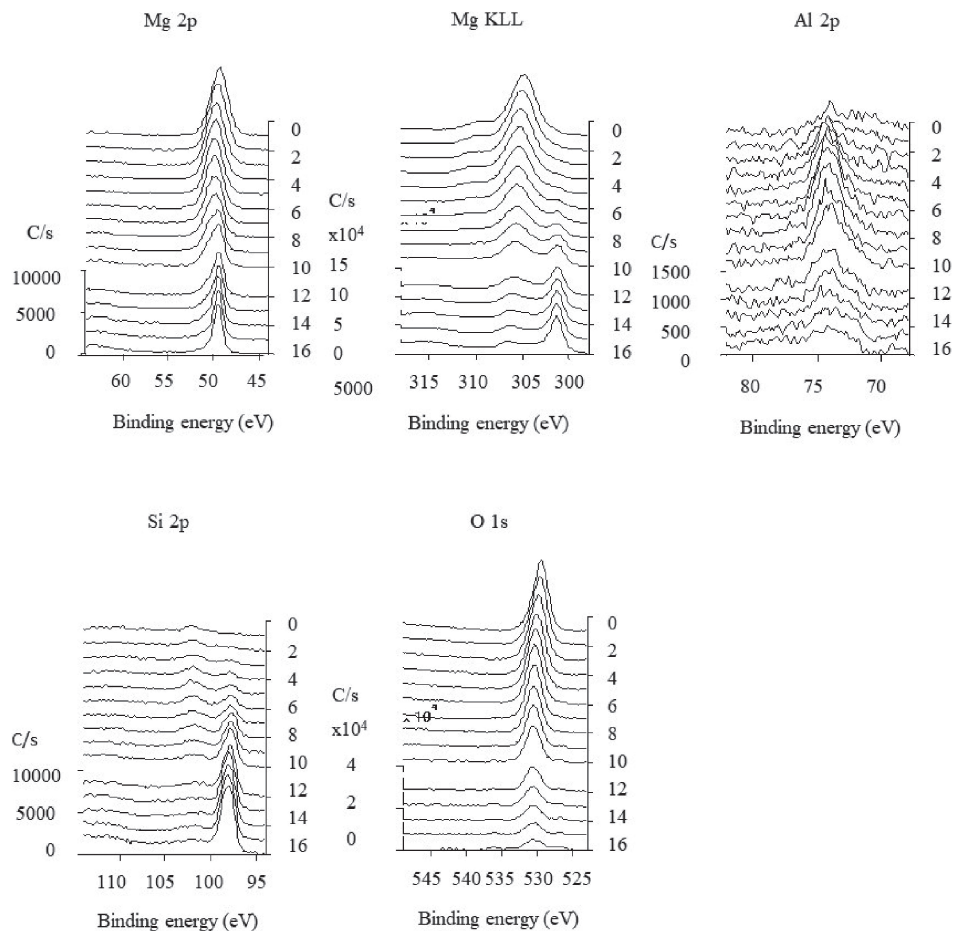

Fig. 7 Binding energy transitions of Mg 2p, Mg KLL, Al 2p, Si 2p, and O 1s the 1st to 16th layers of the sample of Mg_2Si (1.0 at% Sb) + 0.8 mol% α-Al_2O_3, as observed by XPS. The horizontal axis shows the binding energy (eV), the left vertical axis shows the photoelectron intensity (c/s), and the right vertical axis shows the amount of sputtering.

transition layer between MgO and Mg_2Si, C is the segregated layer of aluminum oxide and aluminum, and D is the Mg_2Si matrix. In C, the dark part indicates that the Al concentration is high.

Next, the binding energy transition of each element was evaluated, and the change in the chemical bonding state of each element was investigated. Figure 7 shows the binding energy transition of Mg 2p, Mg KLL, Al 2p, Si 2p, and O 1s of each layer from 1 to 16 layers as revealed by Ar^+ ion etching of the sample of Mg_2Si (1.0 at% Sb) + 0.8 mol% α-Al_2O_3. The graph of the binding energy transition is shown starting from the middle layer, not from the outermost layer, with the 1st layer in the figure corresponding to a depth of 12.5 nm and the 16th layer corresponding to a depth of 31.25 nm. The horizontal axis shows the binding energy (eV), the left vertical axis shows the photoelectron intensity (counts/s), and the right vertical axis shows the etching amount. A binding energy transition from the magnesium oxidation peak of Mg KLL (305.3 eV) to the magnesium metal peak of Mg KLL (301.1 eV) was observed in the eighth layer (22.5 nm from the surface). After the 8th layer, the metal peak became progressively larger while the oxide peak became progressively smaller, becoming very small at the 12th layer (27.5 nm from the surface). The binding energy transition from the magnesium oxidation peak (50.8 eV) to the magnesium metal peak (49.8 eV) due to Mg 2p was not clear (Fig. 7). For Al, a binding energy transition was observed from the aluminum oxidation peak (74.5 eV) to the aluminum metal peak (72.9 eV). Aluminum oxidation peaks were observed in the 1st to 16th layers and aluminum metal peaks were also observed in the 12th to 16th layers, but the peaks were weak. For Si, a silicon metal peak of Si 2p (99.3 eV) appeared from the 5th layer (18.75 nm from the surface), but the peak was weak. The silicon metal peaks then became more prominent toward the interior of the sample. The silicon oxidation peak of Si 2p (103.3 eV) was observed from the 1st to 10th layers but was very weak. For oxygen, an O 1s peak was observed from the 1st layer to the 16th layer, and the intensity of the peak gradually weakened in the deep part of the sample. The above results show that layers containing aluminum oxide and aluminum were formed between the magnesium oxide surface layer and the Mg_2Si matrix.

The binding energy transitions of Mg 2p, Mg KLL, Al 2p, Si 2p, and O 1s in the sample of Mg_2Si (1.0 at% Sb) + 4.5 mol% α-Al_2O_3 were similar to those in Fig. 7.

The reason why Al effectively suppressed the oxidation of Mg_2Si is discussed below. In this study, α-Al_2O_3 powder was mixed with Mg_2Si powder before sintering. As a result, α-Al_2O_3 was reduced to Al by Mg in Mg_2Si particles taking

Table 4　Thermoelectric properties of Mg_2Si with and without added Al_2O_3 or Al.

Sample composition	Thermo-electric property	unit	Temperature(K)				
			373	473	573	673	773
Mg_2Si(1.0at%Sb)	ρ	x10^{-6} (Ω･m)	6.34	6.91	8.16	9.96	12.14
	S	x10^{-4} (V/K)	-1.09	-1.31	-1.53	-1.72	-1.92
	κ	(W/m･K)	7.51	6.22	5.14	4.57	4.31
	ZT		0.09	0.19	0.32	0.44	0.54
Mg_2Si(1.0at%Sb) +2.3 molt% α-Al_2O_3	ρ	×10^{-6} (Ω･m)	5.17	6.25	7.77	9.22	11.07
	S	×10^{-4} (V/K)	-1.21	-1.44	-1.70	-1.83	-1.92
	κ	(W/m･K)	7.53	6.34	5.41	4.81	4.54
	ZT		0.14	0.25	0.38	0.50	0.56
Mg_2Si(1.0at%Sb) + 4.0 at% Al	ρ	×10^{-6} (Ω･m)	4.98	6.12	7.70	9.11	11.17
	S	×10^{-4} (V/K)	-1.07	-1.29	-1.50	-1.66	-1.81
	κ	(W/m･K)	7.10	5.99	5.10	4.58	4.26
	ZT		0.12	0.21	0.33	0.44	0.53

O from adjacent α-Al_2O_3, and the Al then diffused into the Mg_2Si particles during sintering. When Al powder was mixed with Mg_2Si powder before sintering, the Al diffused into the Mg_2Si particles during sintering as well.

When Mg_2Si containing Al is exposed to an oxidizing atmosphere, the following oxidation reaction occurs on the Mg_2Si surface:

$$Mg_2Si\ (s) + 2H_2O\ (g) \rightarrow 2MgO\ (s) + Si\ (s) + 2H_2\ (g)$$

Magnesium oxide is formed as a result of the oxidation of Mg_2Si, and the remaining unoxidized Al and Si diffuse toward the Mg_2Si matrix. If the diffusion coefficient of Al is slightly smaller than that of Si in MgO, the Al may concentrate near the MgO–Mg_2Si interface and react with oxygen diffusing from the surface to form Al_2O_3. Furthermore, the remaining Al also combines with oxygen diffusing from the surface to form stable aluminum oxide, thus preventing the diffusion of oxygen. In this way, a layer containing aluminum oxide and Al is formed between the magnesium oxide surface layer and the Mg_2Si matrix. This layer containing Al_2O_3 would then suppress the internal diffusion of oxygen. Zhang *et al.*[8] showed that an atomic layer of deposited Al_2O_3 coating protects $Mg_2Si_{1-x}Sn_x$ from oxidation in air. In the present study, it appears that the oxidation of Mg_2Si was suppressed by the Al_2O_3 layer rapidly forming at a shallow depth from the surface.

3.3　Thermoelectric evaluation

Table 4 shows the electrical resistivity (ρ), Seebeck coefficient (S), thermal conductivity (κ) and dimensionless figure of merit (ZT) of the samples of Mg_2Si (1.0 at% Sb), Mg_2Si (1.0 at% Sb) + 2.3 mol% α-Al_2O_3 and Mg_2Si (1.0 at% Sb) + 4.0 at% Al. The electrical resistivity decreased in the order of Mg_2Si (1.0 at% Sb), Mg_2Si (1.0 at% Sb) + 2.3 mol% α-Al_2O_3, and Mg_2Si (1.0 at% Sb) + 4.0 at% Al. The absolute value of the Seebeck coefficient was almost the same for Mg_2Si (1.0 at% Sb) + 4.0 at% Al and Mg_2Si (1.0 at% Sb), and that of Mg_2Si (1.0 at% Sb) + 2.3 mol% α-Al_2O_3 was slightly larger than that of the others. The thermal conductivity of Mg_2Si (1.0 at% Sb) + 2.3 mol% α-Al_2O_3 was slightly larger than that of Mg_2Si (1.0 at% Sb) and Mg_2Si (1.0 at% Sb) + 4.0 at% Al, while the thermal conductivity of Mg_2Si (1.0 at% Sb) and Mg_2Si (1.0 at% Sb) + 4.0 at% Al was almost the same. The slightly higher thermal conductivity of Mg_2Si (1.0 at% Sb) + 2.3 mol% α-Al_2O_3 is attributed to the α-Al_2O_3 at grain boundaries because the thermal conductivity of α-Al_2O_3 is about 24 W/m·K at 373 K and 8 W/m·K at 773 K, which are higher

than the corresponding values of Mg_2Si. The obtained ZT values of Mg_2Si (1.0 at% Sb) + 2.3 mol% α-Al_2O were slightly larger than those of the others from 373 K to 673 K, but the difference became small at 773 K. This result suggests that the addition of Al_2O_3 or Al had a slightly positive effect on the thermoelectric properties of Mg_2Si.

Now, let us consider the site in Mg_2Si to which Al diffused. XPS analysis of the binding energy transition of Al 2p shows a small peak near 73 eV inside the oxide layer of Mg_2Si. The energy of this peak indicates the presence of metallic Al. Also, in the measurement of thermoelectric properties, electrical resistance decreased when α-Al_2O_3 or Al was added to Mg_2Si; this is attributed to the replacement of divalent Mg with trivalent Al, which emits electrons. From the above results, it is considered that Al diffused into Mg_2Si and was substituted into Mg sites in the Mg_2Si matrix.

4. Summary

The oxidation behavior of Mg_2Si was evaluated by *in situ* thermal oxidation in a 200 Pa water vapor atmosphere using an E-SEM. The oxidation onset temperature of Mg_2Si (0.5 at% Sb) was 603 K, while that of the Mg_2Si samples with added α-Al_2O_3 or Al was 747 K to 793 K. SEM-EDX analysis and XPS depth analysis before and after thermal oxidation showed that the thickness of the magnesium oxide layer that formed on the surface of samples with added α-Al_2O_3 or Al was about one-tenth that of samples without added α-Al_2O_3 or Al. XPS depth analysis revealed that a layer with a relatively high concentration of aluminum oxide and Al was formed between the magnesium oxide surface layer and the Mg_2Si matrix. The results suggest that a relatively high concentration of aluminum oxide and Al layer suppressed the oxidation of Mg_2Si. The addition of α-Al_2O_3 or Al had a slightly positive effect on the thermoelectric properties of Mg_2Si.

In this study, the sintering temperature and sintering pressure range did not affect the relative density, microstructure, or oxidation-suppressing effect of Mg_2Si with added α-Al_2O_3 or Al.

REFERENCES

1) J. Tani and H. Kido: Intermetalics **15** (2007) 1202–1207.
2) T. Sakamoto, T. Iida, S. Kurosaki, K. Yano, H. Taguchi, K. Nishio and Y. Takanashi: J. Electron. Mater. **40** (2011) 629–634.
3) J. Tani, M. Takahashi and H. Kido: IOP Conf. Ser.: Mater. Sci. Eng. **18** (2011) 142013.
4) D. Stathokostopoulos, D. Chaliampalias, E. Pavlidou, K.M. Paraskevopoulos, K. Chrissafis and G. Vourlias: J. Therm. Anal. Calorim. **121** (2015) 169–175.
5) S. Battiston, S. Boldrini, S. Fiameni, A. Famengo, M. Fabrizio and S. Barison: Thin. Solid Films **526** (2012) 150–154.
6) S.H. Park, Y. Kim and C.Y. Yoo: Ceram. Int. **42** (2016) 10279–10288.
7) P. Nieroda, K. Mars, J. Nieroda, J. Leszczyński, M. Król, E. Drożdż, P. Jeleń, M. Sitarz and A. Koleżyński: Ceram. Int. **45** (2019) 10230–10235.
8) L. Zhang, X. Chen, Y. Tang, L. Shi, G.J. Snyder, J.B. Goodenough and J. Zhou: J. Mater. Chem. A **4** (2016) 17726–17731.
9) K. Fukutani: J. Vac. Soc. Jpn. **56** (2013) 204–209.